Future Technology
Open Access Journal
ISSN 2832-0379

May 2025| Volume 04 | Issue 02 | Pages 76- 91

Journal homepage: https://fupubco.com/futech

https://doi.org/10.55670/fpll.futech.4.2.8

Future Publishing LLC

Article

PNASFH-Net: Parallel NAS forward harmonic Network for colon cancer detection using CT images

V T Ram Pavan Kumar M[1,2]*, Chin-Shiuh Shieh [3], Siva Shankar S[4], Prasun Chakrabarti[5]

[1]PG Dept. of Computer Science & Applications, Kakaraparti Bhavanarayana College (KBN College), Vijayawada, Andhra Pradesh, India
[2]Research Institute of IoT Cybersecurity, Department of Electronic Engineering, National Kaohsiung University of Science and Technology, Taiwan
[3]Department of Electronic Engineering, National Kaohsiung University of Science and Technology, Taiwan
[4]Department of CSE, KG Reddy College of Engineering and Technology, Hyderabad, Telangana, India
[5]Department of Computer Science and Engineering, Sir Padampat Singhania University, India

ARTICLE INFO

Article history:
Received 18 March 2025
Received in revised form
24 April 2025
Accepted 02 May 2025

Keywords:
Median filter, Pyramid Non-local U-Net, Parallel convolutional neural network, Harmonic analysis, Neuron attention stage-by-stage net

*Corresponding author
Email address:
mrpphd2018@kbncollege.ac.in

DOI: 10.55670/fpll.futech.4.2.8

ABSTRACT

Colon cancer is a leading cause of cancer-related deaths worldwide, and early detection is vital to reduce mortality rates. While Deep Learning (DL) models are commonly used for colon cancer detection, they often require large datasets and are time-consuming. To address these challenges, a new model, Parallel Neural Architecture Search Forward Harmonic Network (PNASFH-Net), has been developed. PNASFH-Net begins by preprocessing colon images through Adaptive Median Filtering (AMF) to remove noise. It then segments the affected colon region using Pyramid Non-local U-Net (PNU-Net), optimized by the Remora Shuffled Shepherd Optimization Algorithm (RSSOA)—a hybrid algorithm combining the Remora Optimization Algorithm (ROA) and Shuffled Shepherd Optimization Algorithm (SSOA) for improved segmentation accuracy. Next, features from the segmented images are extracted and analyzed by PNASFH-Net, which combines Harmonic Analysis, Neural Architecture Search Network (NASNet), and Parallel Convolutional Neural Network (PCNN) for accurate detection. Experimental results show that PNASFH-Net achieves 98.345% accuracy, 98.512% specificity, and 98.679% sensitivity, demonstrating its potential for precise and early colon cancer detection.

1. Introduction

Colon cancer remains one of the leading causes of cancer-related deaths worldwide, making early detection crucial for improving patient outcomes. While the importance of early diagnosis is widely recognized, the challenges associated with medical image analysis in this domain are multifaceted and complex. The uncontrolled growth of irregular cells from the body's organs or tissues causes cancer. Cancer cells may develop in various body tissues or organs [1]. Colon cancer is the most frequently detected cancer globally and the second largest source of cancer-related death in men [2]. Metastatic spread is frequently associated with colon cancer, which is an extremely common cancer [3]. Cancer may spread to the colon, which is the longest and largest portion of the large intestine, and the rectum, the shortest portion. There are four sections of the colon, and they include the descending colon, sigmoid colon, rectum, and transverse colon. Growths called polyps can develop in the rectum or colon. Often, these tumors are the first signs of colon cancer. A vital first step in reducing the risk of colon cancer is the recognition and elimination of polyps. Carcinogenic cells develop in the colon or rectum as a result of colon cancer. More lives could have been saved and diseases could have been identified earlier with the use of screening and improved treatment options [4]. The colon cancer cell line HT-29 has an epithelial-like appearance. These cells can be effectively eliminated by the colon cancer chemotherapy medicines 50-fluorouracil and oxaliplatin [5]. Peritoneal carcinosis (PC) is more likely to develop later in life and significantly reduces patient survival times [6]. The survivability of patients with colon cancer can be enhanced by detecting the cancerous lesions in the initial stage, and hence, accurate, reliable diagnosis methods are required [7]. Muscle aches, fatigue, coughing, and other symptoms are common, and these are followed by a variety of syndromes. For the purpose of identifying cancer, radiographic imaging models, including Computed Tomography (CT), Magnetic Resonance Imaging (MRI), Positron Emission Tomography (PET), mammography, histopathological imaging, and ultrasound are often employed. In the event of initial identification, it is also more

difficult to recognize cases because the symptoms are vague and hard to determine [8].

Abbreviations

AI	Artificial Intelligence
AMF	Adaptive Median Filtering
ANN	Artificial Neural Network
CSLBP	Center-Symmetric Local Binary Patterns
CST	Comparative Space Transform
CT	Computed Tomography
CNN	Convolutional Neural Networks
DL	Deep Learning
LBP	Local Binary Patterns
ML	Machine Learning
MRI	Magnetic Resonance Imaging
NASN	Neural Architecture Search Network
PC	Peritoneal carcinosis
PET	Positron Emission Tomography
PN	Pyramid Non-local
ROC	Receiver Operating Characteristic
RSSOA	Remora Shuffled Shepherd Optimization Algorithm
SGD	Stochastic Gradient Descent
SSOA	Shuffled Shepherd Optimization Algorithm
PCNN	Parallel Convolutional Neural Network

Colon cancer detection has been aided by two-dimensional imaging technologies like CT. The detection through CT scan images acquired through radiology methods results in a 20% reduction in the death rate from colon cancer. It has been demonstrated that MRI results produce more accurate results than CT-scanned images; however, the cost of a CT scan is nearly four times lower than that of a Magnetic Resonance Imaging (MRI) [9]. As a result, CT scan images are now more useful for developing countries [10]. Both segmentation and classification are important approaches in the automatic identification of colon cancer. Based on the spatial distribution of tissues in the images, segmentation divides heterogeneous colon samples into homogeneous regions [11]. The use of Machine Learning (ML) in this field has resulted in recent works performing well in detecting colon cancer. Nevertheless, these approaches increase the complexity and time consumption of ML-based cancer detection systems because they require manual feature detection and separate classifiers for detection [12, 13].

The disadvantages of earlier Machine Learning (ML) techniques are addressed mainly by Deep Learning (DL) approaches. These methods use a deep model to integrate the classification and feature extraction phases into a single stage. Typically, the investigators using systems-based DL methodologies established their own deep model or used pre-trained models along with Transfer Learning (TL) methods [14]. Data from videos, high-dimensional images, and anatomical representations can all be analyzed using DL techniques. Likewise, DL techniques use features and hidden attributes from medical images that are not visible to the human eye to help identify cancers early on and differentiate between different stages of the disease [8]. Using DL, researchers improve early detection efforts and acquire insights into development patterns and progression dynamics. The development of algorithms also has the potential for use in medical applications, supporting medical professionals in diagnosing and monitoring cancer [15]. Convolutional Neural Networks (CNNs) achieved high accuracy in the detection of colon cancer [5]. Moreover, CNN techniques have the ability to categorize various varieties of colon cancer with high reliability [16]. Further, pre-trained and pre-designed CNN approaches are often used because of their high performance and accessibility. Besides, various models, namely SqueezeNet, MobileNet, VGGNet (Visual Geometry Group), AlexNet, and so on, have been employed for analyzing medical images, diagnosing various diseases, like brain disorders, lung anomalies, heart abnormalities, and genetic facial diseases [17]. The traditional diagnosis of colon cancer relies heavily on radiologists who manually review imaging studies like CT scans. This approach has several limitations: Radiologists may interpret images differently due to personal experience and biases, leading to inconsistent diagnoses, missed detections, or false positives that can adversely affect patient care. The demanding workload in radiology can cause fatigue, especially when reviewing large volumes of images, which can impair cognitive function and increase the likelihood of diagnostic errors. Tight schedules limit radiologists' time on each case, resulting in rushed evaluations and potential oversight of critical details.

Artificial Intelligence (AI) presents a promising solution by offering consistent, scalable, and objective analysis of medical images, allowing for rapid and accurate data processing that alleviates the burden on radiologists. However, colon cancer poses specific challenges for machine learning models:

- High Intra-Class Variability: The diverse appearances of colon cancer tumours complicate model training, as algorithms must learn to recognize a wide range of cancerous features.
- Ambiguous Boundaries: The difficulty in distinguishing between cancerous and non-cancerous tissues arises from ambiguous boundaries, making accurate segmentation and classification challenging.
- Variability in Image Acquisition Settings: Differences in imaging protocols, equipment, and patient positioning can lead to inconsistencies in image quality, hindering the generalization of machine learning models across diverse datasets.

This work intends to present PNASFH-Net for colon cancer detection based on CT images. Firstly, the input colon image is passed to the AMF in the image pre-processing stage to eliminate the noise. After that, the affected colon region is segmented from the pre-processed image by PNU-Net, which is tuned by the RSSOA model. Here, RSSOA is produced by the integration of ROA and SSOA. Then, feature extraction is performed, and lastly, colon cancer detection is accomplished using PNASFH-Net, which is established by the incorporation of PCNN, NASNet, and Harmonic analysis. The integration of NASNet, PCNN, and Harmonic analysis creates a robust framework for colon cancer detection that leverages the strengths of each component. NASNet's architecture optimization capabilities ensure that the model is well-suited to the complexities of medical imaging, while PCNN enhances feature extraction through parallel processing. Harmonic analysis further enriches the model's ability to detect intricate patterns and textures, ultimately leading to improved diagnostic accuracy. This synergistic approach addresses the unique challenges posed by medical imaging and positions the model to deliver reliable and effective colon cancer detection. The burden associated with treatment approaches, like chemotherapy and/or radiation therapy is reduced when colon cancer is detected early, which also lowers mortality. Finding an anomaly in the tissue becomes a difficult task for pathologists, and hence, to help the pathologist identify the abnormal or normal regions in the colon tissues faster, accurately, and constantly, it is required to develop an imperative and intelligent automated

technique. Hence, this article presents an efficient method for detecting colon cancer called PNASFH-Net. Further, the advantages and disadvantages of several conventional methods for detecting colon cancer.

1.1 Literature review

A method based on K-means was developed for the purpose of detecting colon cancer by Saroja, B., and Selwin Mich Priyadharson, A. [1]. This approach provided better performance and obtained satisfactory results compared to other traditional techniques. But this technique obtained a low accuracy rate. A Deep transfer learning model was developed by Gessert, N., et al. [2] for the classification of colon cancer. Although this technique offered excellent accuracy, the transferability of features was insufficient, and no optimal learning approaches for CLM images were included. Gessert, N., et al. [3] introduced CNN for colon cancer detection. This approach enhanced the performance for the variability of medical learning issues and examined the possibility of identifying malignant tissues. Nevertheless, the identification of malicious tissue in the colon region was not investigated, and this method did not gather additional data. Gupta, P., et al. [4] devised the IR-v2 Type 5 technique for colon tissue classification. This method was faster, robust, and also required less time. Nevertheless, this technique failed to deliberate multi-institutional training and was not evaluated to enhance the robustness of the developed framework.

Sakr, A.S., et al. [5] developed a Lightweight CNN model for colon cancer detection. This technique was more reliable and computationally efficient during the detection process. However, this model did not incorporate any optimization techniques, such as genetic algorithms, for choosing the best features from the deep features that were extracted. Akilandeswari, A., et al. [6] introduced DNN+ResNet 50 for the segmentation and detection of colorectal cancer. This method effectively reduced the amount of manual interaction required and minimized the classification error, which benefited the clinicians. Training a DNN+ResNet-50 model can take a while because of its complicated nature and depth. However, there were overfitting problems with this method. Haq, I., et al. [7] established ResNet-50 for detecting colon cancer. Better performance and faster convergence were the key benefits of this technique, and it also decreased the need for initial training. This technique did not consider additional variations of ML and DL approaches, and it did attain high accuracy. Obayya, M., et al. [8] developed a Biomedical Image Analysis for Colon and Lung Cancer Detection using Tuna Swarm Algorithm with Deep Learning (BICLCD-TSADL) model for colon and lung cancer detection. This model effectively attained the maximum accuracy while demonstrating excellent performance. However, this approach neglected feature fusion and the ensemble learning process, which could have increased the model's effectiveness.

1.2 Challenges

The challenges faced by traditional approaches are listed as:

- In Ref [1], the k-means effectively reduced the features and obtained less computational complexity. Nevertheless, in this technique, a few specific augmented and original images affected the model's reliability.
- In Ref [2], the deep transfer learning method delivered high performance even in small databases. However, this approach was not effective in determining the optimal technique or single transfer strategy for the classification issues.
- In Ref [3], the CNN model obtained better outcomes than various techniques. Nevertheless, this method did not examine a diverse and huge dataset of high-quality CT images, which was important for validating and training DL models.
- In Ref [4], the AI-based IR-v2 Type 5 approach accomplished more accuracy and enhanced classification performance. However, in this technique, the computational burden was very high.
- Several DL algorithms were exploited for addressing medical applications and problems related to health. Nevertheless, these conventional models required a feature extraction process to lessen the information loss. Further, a massive number of samples was also needed for appropriate training, which is considered a challenging task.

2. Proposed PNASF-Net for colon cancer detection

The novelty of the work lies in developing an innovative DL technique named PNASFH-Net, which was developed to detect colon cancer at its initial stage in this research. Firstly, the input colon image is passed to image pre-processing to eradicate the noise. The pre-processing is performed by exploiting AMF. Incorporating self-supervised learning techniques into PNASFH-Net [19], alongside the use of Adaptive Median Filtering (AMF) for noise reduction, can significantly enhance the model's performance on colon cancer detection tasks. The comparisons with advanced methods like Non-Local Means filtering and wavelet-based noise reduction demonstrate AMF's superior ability to preserve fine details while effectively reducing noise, making it particularly well-suited for pre-processing colon cancer CT images. Following this, the affected colon region is segmented using PNU-Net [10], which is trained using the RSSOA algorithm. Moreover, the RSSOA approach is formed by integrating ROA [11] and SSOA [12]. After this, feature extraction is performed, where several features, namely Convolutional Neural Network (CNN) [13], Local Vector Pattern (LVP) [14], and Center-Symmetric Local Binary Patterns (CSLBP) [15] are mined. At last, colon cancer detection is executed using a DL network termed PNASFH-Net, which is devised by the combination of Parallel Convolutional Neural Network (PCNN) [16], NASNet [17], and Harmonic analysis [18]. Figure 1 exhibits the structural representation of PNASFH-Net for colon cancer detection.

2.1 Image acquisition

Assume that the input colon image is taken from a dataset [20] for detecting colon cancer, and the dataset is formulated as:

$$X = \{X_1, X_2, \ldots, X_a, \ldots, X_y\} \quad (1)$$

Here, y exemplifies the overall quantity of images, and Xa epitomizes the a^{th} image, which is utilized for colon cancer detection.

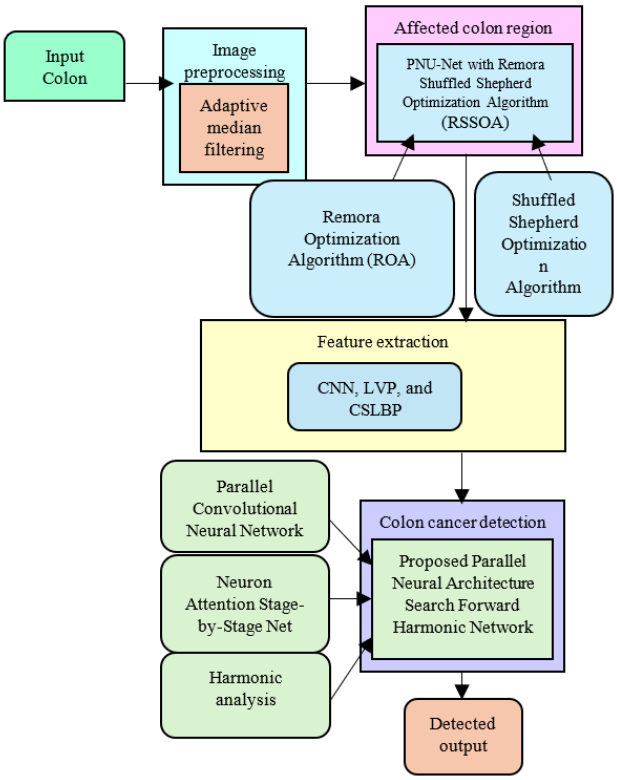

Figure1. Structural representation of PNASFH-Net for colon cancer detection

2.2 Image Pre-processing

Image pre-processing is measured as an important task in increasing the image quality, which is employed to enhance the performance, accuracy, and reliability of outcomes in several areas, namely remote sensing, medical imaging, and so on. The major aim is to maximize the overall performance by enhancing the quality of the image. Here, AMF [9] is employed for pre-processing the input image Xa. AMF is more applicable for images with high levels of salt-and-pepper noise. When the salt-and-pepper noise in the image is high, it is essential to improve the filtering template's size, and the window size can be adaptively adjusted by the AMF process. AMF is used for identifying the points of noise and has the ability to correct the size of the template by determining the finest template. Further, the outcome from image pre-processing is exemplified as $\hbar_t$.

2.3 Affected colon region segmentation

In medical imaging, affected colon region segmentation plays a crucial role. To precisely identify and describe irregular regions in colon images, progressive image analysis approaches are required. Moreover, segmenting the affected colon region is used to locate the particular area of the colon in the image that shows illnesses or abnormalities. Here, the affected colon region is segmented from the pre-processed image $\hbar_t$by utilizing PNU-Net [10], described below.

2.3.1 Architecture of PNU-Net

The PNU-Net technique is utilized for segmenting the affected colon region, which is done by taking the pre-processed image $\hbar_t$ as input. At first, convolutional (Conv) layers are exploited for mining the local features and then, the cancer-affected region detection is converted into the segmentation of the affected region's local neighborhood for addressing the challenges in affected colon region segmentation. Moreover, U-Net is introduced, which is a robust and simple baseline network for learning local morphological features and for segmenting the local neighborhood. Next, global structural features are captured for the estimation of the better local neighborhood, which is performed using a non-local module. Further, in order to minimize the consumption and computation problems, a Pyramid Non-local (PN) with pyramid sampling is employed. Pyramid sampling involves creating multiple scales of the input image, allowing the network to process features at different resolutions. By analyzing the image at various scales, PNU-Net can capture both fine details and broader contextual information without significantly increasing the computational burden. This approach reduces the number of parameters and computations required compared to fully convolutional networks that operate at a single scale, thus enhancing efficiency while maintaining the ability to discern important features across different spatial hierarchies**.** By incorporating non-local operations, PNU-Net can effectively capture long-range dependencies, which is crucial for identifying abnormal regions in medical images. This capability allows the model to consider the broader context when making segmentation decisions, leading to more accurate delineation of affected areas. The ability to integrate information from distant pixels enhances the model's understanding of the overall structure and context of the image. This is particularly important in complex medical images where the presence of noise or artifacts can obscure local details. Non-local operations help mitigate these issues by providing a more holistic view of the image.

a) **Task conversion**: Even with pathological deformity and temporal diversity, the affected region holds global structural and local morphological features. Hence, local neighborhoods all over the affected colon region may be regarded as a robust identification of the affected region. Here, a circular image patch positioned at the affected region with radius g is extracted, where g is adequately huge for visually identifying the cancerous region. In the training process, the network is trained for segmenting the affected regions' local neighborhood area D. Thus, colon detection is converted into segmentation of the cancer-affected region's local neighborhood area D, and it is modeled as:

$$D=\{m\}(||m-W||\leq g) \quad (2)$$

Consequently, the cancer-affected region W' is to be identified at the centroid of the segmentation mask D', expressed as:

$$W'=R[D']=(\sum_u m_u)/k \quad (3)$$

Moreover, the local neighborhood area D with a large g value produces local features, which can be more robust for segmenting the cancerous region with abnormalities, k implies a number of pixels.

b) **Local-Global feature learning**: Here, cancer-affected region detection is converted into an affected area segmentation task, and then U-Net, which is a strong segmentation network, is employed for learning the local features and for segmenting the local neighborhood. U-Net comprises a skip connection, decoder, and encoder for performing segmentation. Further, PN is utilized for learning long-range features, which is done by calculating the response

at a location as the weighted quantity of features at each location is expressed as:

$$\sigma_u = \frac{1}{V(j)} \sum_{\forall d} h(j_u, j_d) n(j_d) \quad (4)$$

where the output and input feature is symbolized as σ and j, the output index is epitomized as u, the index that computes every possible location is specified as d, h, and n indicates pairwise and unary functions. Here, the representation is computed by a unary function and then normalized by V(j). In order to convert the input feature G∈$Re^{E\times\beta\times J}$ to value branch l, key branch ϕ, and query branch φ, with size Eˆ×β×J, three 1×1 convolutions (Conv) are employed. Here, the input feature map's width and height are symbolized as and, and the channel number of the input feature is represented as Eˆ. After this, a similarity matrix $S \in Re^{\zeta\times\zeta}$ is obtained by matrix multiplication of the query branch ϕ , and it is signified as:

$$S = \varphi^T \times \phi \quad (5)$$

Here, ζ characterizes the number of nodes. In value branch l, for each position, the outcome from the attention layer is attained using matrix multiplication based on the similarity matrix, and it is represented as:

$$A = S \times \ell^T \quad (6)$$

Here, A∈$Re^{\zeta\times\hat{E}}$, the pixel-level pairwise relationship among every location conveys memory and excessive computation for the non-local component is written as O(Eˆς^2)=O(Eˆβ² J²). In order to solve excessive computation of the non-local module, PN with pyramid sampling is implemented to reduce consumption and computation issues. Moreover, limited representative points from ϕ and l are sampled using pyramid sampling. Here, the time complexity of the PN model is O(Eˆςα), where the quantity of sampled anchor points is signified as α. Further, to optimize the segmentation of mask D, the dice coefficient is utilized, and the segmented output is designated as ξ. Figure 2 portrays the architecture of PNU-Net.

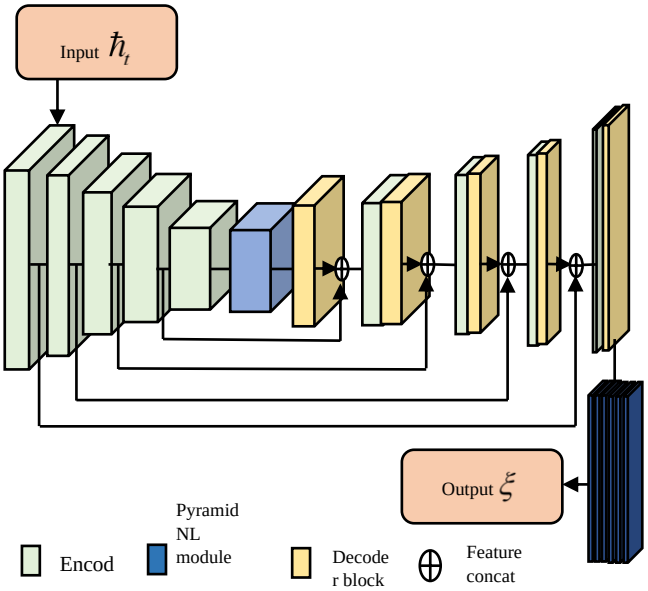

Figure 2. Architecture of PNU-Net

2.3.2 Training PNU-Net using RSSOA

The PNU-Net is tuned by employing the RSSOA technique, which is engineered by the incorporation of ROA [11] and SSOA [12]. Here, ROA [11] is stimulated based on the parasitic behavior of remora, which is a species of marine fish. The exploitation and exploration are categorized into two processes, namely eat thoughtfully and free travel, which is performed by inspiring the entire process of predation of the remora. Here, the switching among the phases is done in terms of Remora's experience, and it is collected by utilizing an experimental attack. Moreover, ROA is more efficient in maintaining high experimental ability, and it has the ability to solve various engineering and optimization problems. Further, SSOA [12] is inspired by the shepherd's behavior, which employs an animal's instinct to determine the optimal pasture. This technique is capable of finding the best solution with a few evaluations, and it has the capability to obtain a high accuracy rate. The main intention of this method is to enhance performance by amalgamating SSOA and ROA. The updated equation of RSSOA is given as:

$$F_{a'}^{s+1} = \left(\frac{(2-rand(0,1))}{2(\rho\times rand-1)+rand(0,1)}\right)\left(F_{rand}^{s} \times \rho \times rand - F_{a'}^{s}(1 - rand \circ (\rho + \varpi)) + \varpi \times rand \circ F_{n'}^{s}\right) \quad (7)$$

Here, the current solution is specified as $F_{a'}^{s}$, the random value between [0,1] is designated as *rand*, the solution vectors of sheep and horse selected are symbolized as $F_{n'}$element-wise multiplication is characterized as ∘, parameters are mentioned as ρ and ϖ, F_{rand} denotes random position.

2.4 Feature extraction

Feature extraction is employed to identify and extract data or features from the segmented image ξ. In image analysis, feature extraction is utilized to capture and represent the key patterns or features in an image. It is also vital to transform the images into the required format, which is done for decision-making tasks and subsequent analysis. Moreover, the features are mined for improving the performance by decreasing the complexity, and this process is performed by taking ξ as input. Furthermore, the features, including LVP, CNN, and CSLBP, are mined, and these features are described below.

2.4.1 CNN

CNN [13] is one of the types of Deep and feed-forward Artificial Neural Network (ANN). CNN consists of three layers, namely pooling, Conv, and Fully connected. Conv is regarded as the first layer, which is used for mining several feature representations from an input image. Next, the pooling layer is exploited to lessen over-fitting issues and computation cost by improving the model's performance. Subsequently, the fully connected layer is exploited to combine the features from the former layer. Here, the CNN feature is obtained from the conv layer and is represented as U_1

2.4.2 LVP

LVP [14] is used for minimizing the feature length, and it is carried out by eliminating the redundant data from the segmented image. Here, each pixel's vector is produced by Comparative Space Transform (CST), which is performed by identifying the values among adjacent and target pixels. Moreover, LVP is employed for providing several pairwise directions of the vector of nearest and referenced pixels. To obtain a robust micropattern structure, pairwise orientation is used, and the expression of LVP is written as,

$$U_2 = LVP_{\kappa,\tau}(\delta_{m'}) = \{LVP_{\kappa,\tau,e}(\delta_{m'}) | e = 0°, 45°, 90°, 135°|\} \quad (8)$$

where, exemplifies index angle related to orientation variations, τdenotes radius, δ(m')characterizes target pixel, k specifies adjacent pixels, and U_2 epitomizes the LVP feature

2.4.3 CSLBP

CSLBP [15] is a modified version of Local Binary Patterns (LBP) employed to solve the overfitting issues. CSLBP enhances traditional LBP by addressing overfitting issues and improving texture recognition by focusing on center-symmetric pixel relationships. This method allows for a more robust representation of textures, making it particularly effective in medical imaging applications where distinguishing subtle differences in tissue textures is crucial for accurate diagnosis and treatment planning. By leveraging the spatial relationships between pixels, CSLBP provides a more comprehensive understanding of the underlying texture patterns, leading to improved performance in detecting abnormalities in colon tissues. Moreover, CSLBP is used to capture gradient information better than LBP, and here, gray-level differences among center-symmetric pairs of nearest contradictory pixels are associated as an alternative to the gray-level of every pixel with a center pixel. This feature is employed for improving the discriminatory power of LBP, and thus CSLBP captures texture data that is connected to spatial and symmetry relations among pixels. The CSLBP feature is modeled as,

$$U_3 = CSLBP_{\kappa,\tau,w}(d_{t'}^{'}, g_{t'}^{'}) = \sum_{\iota=0}^{\frac{\chi}{2}-1} \zeta\left(\lambda_\iota - \lambda_{\iota+(\frac{\chi}{2})}\right)^{2^\iota} \quad (9)$$

$$\lambda(d^{'}) = \begin{cases} 1, d^{'} > w \\ 0, otherwise \end{cases} \quad (10)$$

Here, the amount of nearest pixels is signified as κ, the radius is implied as τ, the nearest pixel's value is denoted as $\lambda\ \iota$, and mentions the small value employed for enhancing the robustness of CSLBP, and the CSLBP feature is epitomized as U_3.

Furthermore, the entire feature vector Uis generated by considering the above-mentioned features and is expressed as,

$$U=\{U_1,U_2,U_3\} \quad (11)$$

2.5 Colon cancer detection

The colon is considered the largest organ in the large intestine, and this cancer leads to death. This cancer is also regarded as the most commonly occurring cancer all over the world. Moreover, colon cancer occurs due to various reasons, such as a lack of fruit intake, chain-smoking, and heavy intake of fats and meat. Therefore, this cancer must be treated early by identifying it at the initial stage to reduce the burden and mortality rate. While modern transfer learning approaches like Efficient Net offer valuable capabilities, their limitations in fine-tuning on small, specific datasets, potential domain shifts, and the complexity of medical data make them less suitable for colon cancer detection. The need for a tailored approach that can adaptively learn from the unique characteristics of colon cancer CT images led to the selection of a more specialized framework, combining NASNet, PCNN, and Harmonic analysis, which collectively address the specific challenges of this domain. Thus, PNASFH-Net is used for colon cancer detection, where PNASFH-Net is formed by the fusion of PCNN [16], NASNet [17], and harmonic analysis [18]. Moreover, PNASFH-Net includes three modules, such as PCNN, NASNet, and PNASFH-Net layer. The multiplication of pre-processed image $\hbar_t$ with weight Q_1 is executed initially, and the resultant output B1 is normalized. At the same time, pre-processed image $\hbar_t$is passed to NASNet, and the obtained outcome is multiplied by the normalized output $\sum Q_1\hbar_t$ to attain B_1Alternatively, the extracted feature U is fed to NASNet, and the output produced is multiplied by a weight Q_2 and then by the NASNet output B_1 to obtain the outcome B2. Lastly, the outcomes B_1 and B_2 are combined by Harmonic analysis [24] to obtain the final colon cancer detection outcome B3. Figure 3 signifies the general outline of the PNASFH-Net for colon cancer detection.

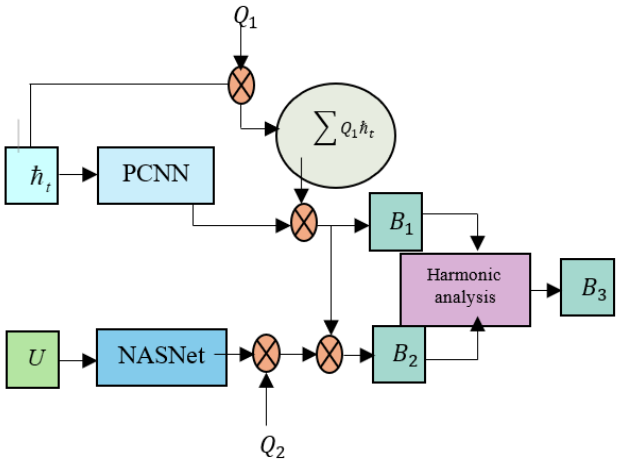

Figure 3. General outline of PNASFH-Net for colon cancer detection

2.5.1 PCNN model

In PCNN [16], the pre-processed image $\hbar_t$is taken as input, and here CNN methods are parallelized by utilizing the concept of data parallelism. Furthermore, parallel tuning is utilized for creating similar outcomes as sequential tuning, and Stochastic Gradient Descent (SGD) is used to tune the CNN. Moreover, PCNN can efficiently lessen the scaling problems, and it has two significant features, such as first, gradient parameters are pooled, and then they are lessened across every node by means of asynchronous communications. Next, gradient computations are simulated in a few fully connected layers. Here, a set of variables is employed to represent the data. Here, the depth of the feature maps at output/input are implied as p_2/p_1, the total images is mentioned as Z, and the count of row/column filters is typified as Ω_3/O_3The quantity of output/input neuron columns is symbolized as L2/L1, the total neurons in the bottom/current layers is specified as Gbot',Gcur', and the measure of output/input neuron rows is designated as Ω_2/Ω_1. Additionally, fully connected and Conv layers are regarded as two varieties of widespread layers in CNN. Here, in Conv,image2Col is utilized for reallocating the input data, and it is done by changing the computation pattern to matrix multiplication. Next, in the fully connected layer, the computation pattern is also similar to matrix multiplication, and the computation workload is considered as a group of data transformations and matrix multiplication. The functions used for data transformation are represented as *Col2image* and *image2Col*, which are used in open-source structures. The filter's size is stimulated using image2col into columns, and they are incorporated to produce a two-dimensional matrix. To transfer the column to blocks of the original data layout, col2image is used. Besides, PCNN is employed for changing a massive volume of data in input activation to the single large matrix.

In the feed forward, the Conv layer's input is obtained from the input saved in a row. All mini-batches of Zimages are produced into a dimensional matrix Z×p_1 Ω_1 L_1, and then converted by *image2col* into G_1' Ω_3 L_3×ZΩ_2 L_2 matrix. After this, the weight matrix p_2×p_1 Ω_3 Ω_2 is multiplied and the bias vector p_2 is added to the matrix, and the outcome of the activation matrix p_2×p_2 Ω_2 Ω_2 is modelled as:

$$M^{v-1} = image2col(R'^{v-1}) \quad (12)$$

The output in PCNN is expressed as:

$$C = R'^{v} = F'(E'^{v}\hbar_t + \eta^{v}) \quad (13)$$

Here, F' epitomizes activation function, Q_1 symbolizes weight, bias is quantified as η, M indicates matrix designed by *image2col*, output from PCNN is embodied as C, γ×$p_1\Omega_1L_1$ and p_1×γΩ_1L_1 typifies generation of image2col, R'^{v} designates activation matrix at v^{th} layer. Figure 4 illustrates the architecture of PCNN.

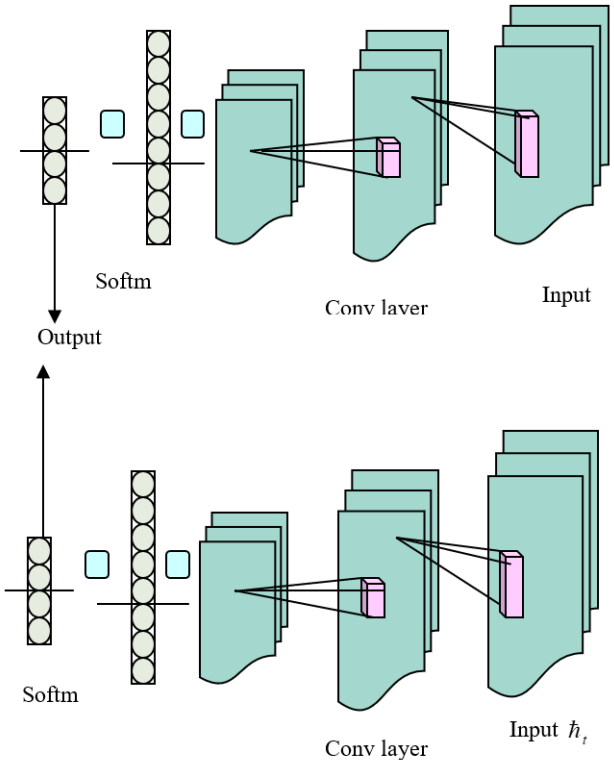

Figure 4. Architecture of PCNN

The output from PCNN is multiplied by the normalized output $\sum Q_1$ $\hbar_t$ for attaining B_1, and it is signified as:

$$B_1 = F'(E'^{v}\hbar_t + \eta^{v}) * \sum\sum(Q_1\hbar_t) \quad (14)$$

2.5.2 NASNet model

The NASNet approach [17] is a new framework formulated by the integration of Auto ML and Neural Architectural Search (NAS). Here, the network's efficiency is enhanced by executing several modifications in terms of the regularization quantity of layers, weights, techniques, and so on. Moreover, NASNet has high network capacity and generalizability, which is used for enhancing the sensitivity of data during the process. Further, NASNet has the capability to efficiently overcome the problems that are experienced by several networks during the process of large datasets by creating building blocks for small to large datasets. This approach includes Conv cells, such as reduction and normal cells, used for classification tasks. Here, the extracted feature U is fed as input to NASNet. Generally, a softmax function is employed in NASNet, and it is articulated by the expression given as:

$$T^r = \omega(U) \quad (15)$$

Here, ω(U)is mentioned as,

$$\omega(U) = \frac{exp^{U}}{\sum_{c=1}^{Y} exp^{U^c}} \quad (16)$$

where *exp* specifies the standard exponential function, vector activation component is implied as Tr, the overall quantity of classes is typified as Y, and $\sum^{U}$ epitomizes probability distribution. Further, two metric spaces, namely L'and A'are considered, and here the target function μ:L'→A' postulates a limited aggregate of points μ(L'^{1}),μ(L'^{2}),μ(L'^{3}),...,μ(L'^{8}) for identified labelsε^1,ε^2,ε^3,...,ε^8. Besides, metric space L' is alienated into various modules, and after this, one-hot encoding is applied, which is expressed as

$$\varepsilon_c[v \in L'|\mu(v) = c] \qquad \text{at } c \in \{1,2,3,\dots,8\}: L' = \cup_{c=1}^{8}\varepsilon_c \quad (17)$$

In order to describe the process performed in neural network, target function discrimination μ:L^'→A^'amongst numerous class labels is executed, and it is designated as,

$$T_{h'}^{r} = \omega\left(\sum_{o=1} P_{h'o}^{r} T^{r-1} + x_{h'}^{r}\right) \quad (18)$$

Here, o and h' exemplify rows and columns of the matrix, P and x represent the weight and bias of the r^{th} layer. The vectorized form of equation (18) is mentioned as,

$$I = T^r = \omega\left(\sum_{j'} P^r U + x^r\right) \quad (19)$$

Here, U indicates extracted feature, I characterizes outcome from NASNet. Figure 5 embodies the architecture of NASNet.

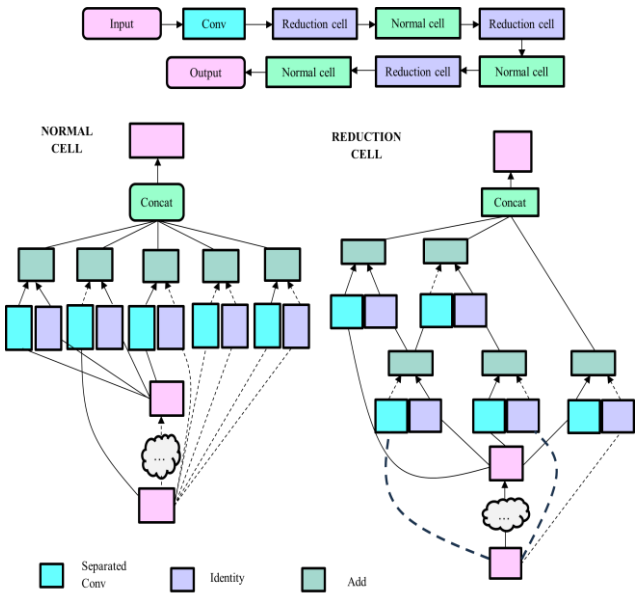

Figure 5. Architecture of NASNet

The attained outcome is multiplied by weight Q_2 and then by B_1 to obtain outcome B_2, which is expressed as

$$B_2 = \omega\left(\sum_{j'} P^r U + x^r\right) * Q_2 * [F'(E'^{v}\hbar_t + \eta^v) * \sum\sum(Q_1\hbar_t)] \quad (20)$$

2.5.3 PNASFH-Net layer

In the PNASFH-Net layer, the outcomes from PCNN and NASNet are fused using harmonic analysis to detect colon cancer. Harmonic analysis [13] is evaluated by contemplating long-term forecasting ability for actual time series, which offers complicated functions to be categorized as incorporations of modest periodic functions. Furthermore, the time series technique is combined with PCNN and NASNet for estimating the unidentified deterministic components from fusion methods by multiple-test procedures. The periodical structure for time series is articulated as:

$$q_{(1)}, q_{(2)}, \ldots, q_{(z)}, \ldots, q_{(l)} \quad (21)$$

Here, length is implied as *l*, and $q_{(z)}$ characterizes the z^{th} time series data considered for observation, and it is expressed as:

$$q_{(z)} = \upsilon_0 + \sum_{w'=1}^{b'}\left(\upsilon_{w'} cos\left(\frac{2\pi w' z}{l}\right) + f_{w'} sin\left(\frac{2\pi w' z}{l}\right)\right) \quad (22)$$

where total cycles are represented as w', υ , and f designates a preselected constant. Further, assume *l=2* and *b'=1*, then equation (22) becomes**:**

$$q_{(z)} = \upsilon_0 + \upsilon_1 cos\left(\frac{2\pi z}{2}\right) + f_1 sin\left(\frac{2\pi z}{2}\right) \quad (23)$$

$$q_{(z)} = \upsilon_0 + \upsilon_1 cos(\pi z) + f_1 sin(\pi z) \quad (24)$$

Where

$$\upsilon_0 = \frac{1}{l}\sum_{z=1}^{l} q_z \quad (25)$$

$$\upsilon_0 = \frac{1}{2}\left[q_{(1)} + q_{(2)}\right] \quad (26)$$

$$\upsilon_{w'} = \frac{2}{l}\sum_{z=1}^{l} q_z cos\left(\frac{2\pi w' z}{l}\right) \quad (27)$$

As we have considered w'=1 and l=2, the above equation becomes:

$$\upsilon_1 = \frac{2}{2}\left[q_{(1)} cos\left(\frac{2\pi}{2}\right) + q_{(2)} cos\left(\frac{2\pi 2}{2}\right)\right] \quad (28)$$

$$\upsilon_1 = q_{(1)} cos(\pi) + q_{(2)} cos(2\pi) \quad (29)$$

$$\upsilon_1 = q_{(1)}(-1) + q_{(2)}(1) \quad (30)$$

Further

$$f_{w'} = \frac{2}{l}\sum_{z=1}^{l} q_{(z)} sin\left(\frac{2\pi w' z}{l}\right) \quad (31)$$

When w'=1 and l=2, we get

$$f_1 = \frac{2}{2}\left[q_{(1)} sin\left(\frac{2\pi}{2}\right) + q_{(2)} sin\left(\frac{2\pi 2}{2}\right)\right] \quad (32)$$

$$f_1 = q_{(1)} sin(\pi) + q_{(2)} sin(2\pi) \quad (33)$$

$$f_1 = q_{(1)}(0) + q_{(2)}(0) \quad (34)$$

Moreover, the time series model is considered as q(z-1),q(z) and q(z-1), thus we get

$$\left.\begin{aligned} q_{(1)} &= q(z-1) \\ q_{(2)} &= q(z) \\ q_{(3)} &= q(z+1) \end{aligned}\right\} \quad (35)$$

Substituting equation (35) in equations (24), (26), (30), and (34), we get

$$q(z+1) = \upsilon_0 + \upsilon_1 cos(\pi z) + f_1 sin(\pi z) \quad (36)$$

$$\left.\begin{aligned} \upsilon_0 &= \frac{1}{2}[q(z-1) + q(z)] \\ \upsilon_1 &= -q(z-1) + q(z) \\ f_1 &= 0 \end{aligned}\right\} \quad (37)$$

By substituting equation (37) in equation (36), we get

$$q(z+1) = \frac{1}{2}[q(z-1) + q(z)] + (-q(z-1) + q(z))\, cos(\pi z) + 0 \quad (38)$$

$$q(z+1) = \frac{1}{2}q(z-1) + \frac{1}{2}q(z) - q(z-1)\, cos(\pi z) + q(z)\, cos(\pi z) + 0 \quad (39)$$

$$q(z+1) = q(z-1)\left[\frac{1-2\, cos(\pi z)}{2}\right] + q(z)\left[\frac{1+2\, cos(\pi z)}{2}\right] \quad (40)$$

Consider q(z-1)=B_1, q(z)=B_2, and q(z+1)=B_3. By applying these values in equation (40), we get

$$B_3 = B_1\left[\frac{1-2\, cos(\pi z)}{2}\right] + B_2\left[\frac{1+2\, cos(\pi z)}{2}\right] \quad (41)$$

Furthermore, by substituting the values of B_1 and B_2, equation (41) becomes

$$B_3 = \left(F'(E'^{v}\hbar_t + \eta^v) * \sum\sum(Q_1\hbar_t)\right)\left[\frac{1-2\, cos(\pi z)}{2}\right] + \left(\omega\left(\sum_{j'} P^r U + x^r\right) * Q_2\right)\left[\frac{1+2\, cos(\pi z)}{2}\right] * [F'(E'^{v}\hbar_t + \eta^v) * \sum\sum(Q_1\hbar_t)] \quad (42)$$

Here, $E'^{v}$and $\eta^{s'}$ represents the weight and bias of v^{th}layer from PCNN, x^r and P^r exemplify the bias and weight of r^{th}layer from NASNet, U indicates extracted feature, $\hbar_t$ epitomizes the preprocessed image, and B_3 denotes the detected output attained by the PNASFH-Net.

3. Results and discussion

The outcomes acquired from the experiment by PNASFH-Net employed for colon cancer detection and the discussions done to assess the efficiency of PNASFH-Net are elucidated below**:**

3.1 Experimental setup

The execution of PNASFH-Net for colon cancer detection is performed employing the Python tool using CT colonography databases [20].

3.2 Dataset description

CT Colonography [20] is the dataset that was used in the experimentation. There are 941,771 images in the dataset that were obtained using CT modalities from 825 individuals. Besides, XLS sheets including data on the polyps, including a description and locations within the colon segments, are also present. Three XLS sheets, one for each size polyp (larger than 10 mm), smaller polyps, and no polyps, are contained in the dataset. The dataset contains the supine and prone DICOM images**.**

3.3 Performance metrics

Several performance metrics are used to assess PNASFH-Net's efficacy in detecting colon cancer. These metrics are elucidated below.

a) Accuracy

The ratio of images that the PNASFH-Net correctly classifies to the overall images applied is known as the accuracy, and it is signified by,

$$Accuracy = \frac{H_{tp}+H_{tn}}{H_{tp}+H_{tn}+H_{fp}+H_{fn}} \quad (43)$$

wherein, H_{tn} indicates true negative, false negative is specified by H_{fn},H_{tp}epitomizes true positive and H_{fp}postulates a false positive.

b) Sensitivity

Sensitivity is the measure of positivity and is represented by the true positivity rate (TPR). Moreover, the computation for sensitivity is stated below,

$$Sensitivity = \frac{H_{tp}}{H_{tp}+H_{fn}} \quad (44)$$

c) Specificity

Specificity is measured by the True Negative Rate (TNR), which can be found by applying the expression below:

$$Specificity = \frac{H_{tn}}{H_{tn}+H_{fp}} \quad (45)$$

d) Confusion matrix

The actual and predicted classifications generated by any classifier are shown in a confusion matrix. The predicted labels or classes are represented in the columns of a confusion matrix, while the actual labels or classes are represented in the rows.

e) Receiver Operating Characteristic (ROC) curve

A visual representation of the relation between the TPR and FPR is called an ROC curve.

f) Loss curve

A neural network's training process is illustrated by a graphical plot called a loss curve, which shows the relationship between the number of epochs and the training loss or error.

g) Memory usage

Memory usage is the metric that quantifies the total amount of RAM utilized by the model during its execution. It is measured in MegaBytes(MB).

3.4 Image results

Figure 6 discusses the experimental outcomes of the newly introduced PNASFH-Net. In Figures 6a and 6b, the input and preprocessed images are indicated. The segmented image is shown in Figure 6c. Also shown in Figures 6d and 6e are the LVP and CSLBP-feature extracted images.

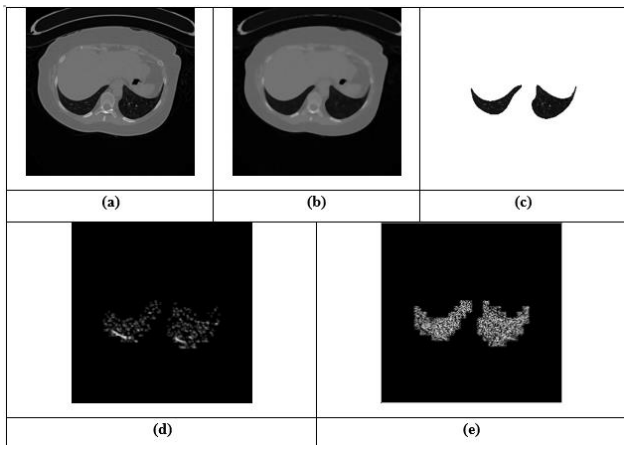

Figure 6. Image results of PNASFH-Net for colon cancer detection concerning, a) Input, b) preprocessed, c) segmented, d) LVP feature extracted, and e) CSLBP feature extracted images

3.5 Segmentation methods

Various methods, like ALTER-ATTUNET [21], UNETR network [22], SegChaNet [23] are employed for comparing the performance of the proposed PNU-Net_RSSOA used for segmenting the affected colon region.

(i) Segmentation analysis

The valuation of segmentation accuracy using different training sets and k-values is shown in Figure 7. The evaluation of segmentation accuracy with the training set is exhibited in Figure 7a. The segmentation accuracy of ALTER-ATTUNET is 85.009%, UNETR network is 87.788%, SegChaNet is 90.998%, and the proposed PNU-Net_RSSOA is 93.779% when considering the training set is 90%. The effectiveness of PNU-Net_RSSOA is enhanced by 9.35%, 6.39%, and 2.97%. Figure 7b indicates the examination of segmentation accuracy by varying k-values. The segmentation accuracy acquired by ALTER-ATTUNET, UNETR network, SegChaNet, and proposed PNU-Net_RSSOA is 87.900%, 89.009%, 91.998%, and 94.179% for k-value is 9. The effectiveness of PNU-Net_RSSOA is improved by 6.67%, 5.49%, and 2.32%.

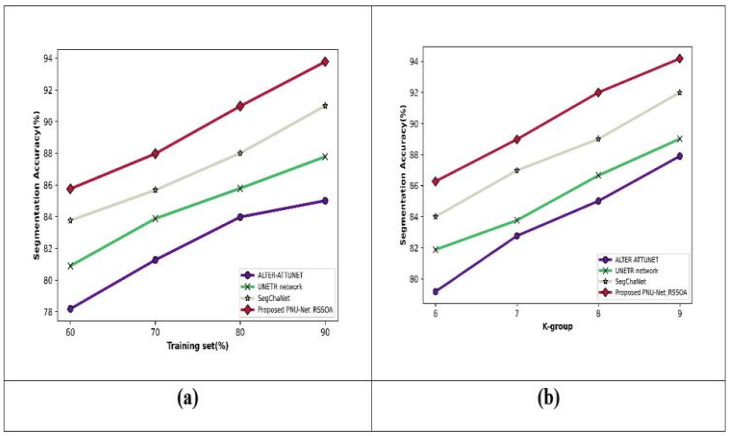

Figure 7. Assessment of PNU-Net_RSSOA based on segmentation accuracy by changing a) the training set and b) the K-value

3.6 Comparative techniques

The performance of the PNASFH-Net technique is assessed by comparing it with the conventional models, including RSSOA-CNN based transfer learning, Vision transformer, Dragonfly Water Wave Optimization-based deep Recurrent Neural Network (DWWO-based deepRNN), Convolutional Neural Network (CNN) [3], Deep transfer learning [2], and K-Means [1].

3.7 ROC curve

The ROC curve's goal is to determine the ideal threshold value for enhancing the classifier's performance. A prediction outcome of a confusion matrix is represented by each point in the ROC space. Figure 8 shows the graph between TPR and FPR. By considering FPR as 0.8, the TPR computed by K-Means is 0.920, Deep transfer learning is 0.932, CNN is 0.956, DWWO-based deepRNN is 0.967, and RSSOA-CNN-based transfer learning is 0.980, while the proposed PNU-Net_RSSOA attained a TPR of 0.990.

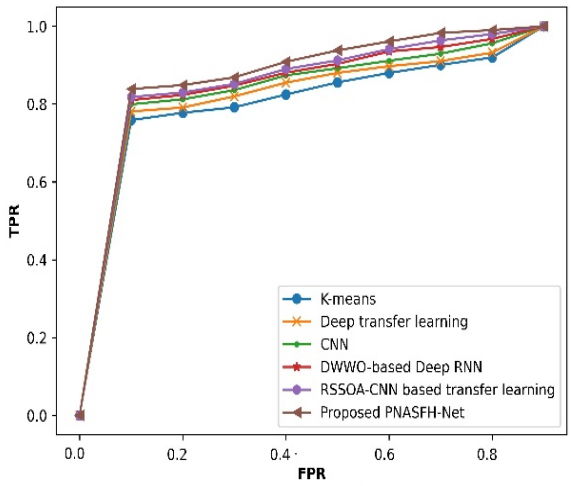

Figure 8. Assessment based on the ROC curve

3.8 Loss curve

The loss curve for the PNASFH-Net method is shown in Figure 9. It is demonstrated that the PNASFH-Net can learn quickly, and it yields a substantial reduction in training loss when the number of epochs is changed from 0 to 140.

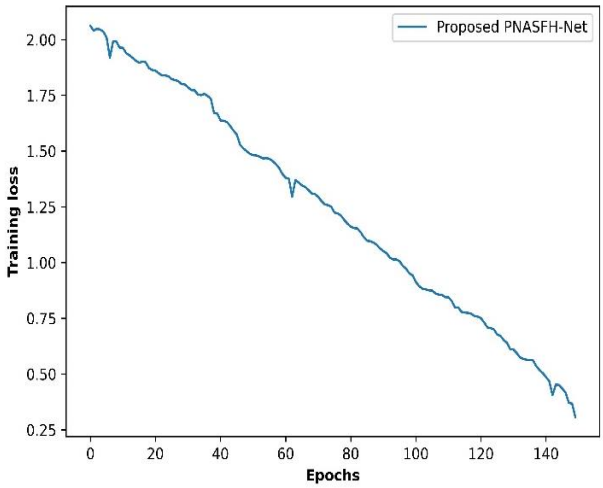

Figure 9. Loss curve of the PNASFH-Net technique

3.9 Confusion matrix

Figure 10 shows the confusion matrix of PNASFH-Net. The figure shows that the classifier performs well in detecting colon cancer. The classifier correctly predicted 362 outcomes out of 400 outcomes. Further, only 6 cases were detected wrongly as positives, and 32 samples were detected wrongly as colon cancer. Three hundred thirty samples were correctly found as cancer cases, and 32 were normal cases.

3.10 Comparative analysis

Various evaluation metrics based on the training set and k-group are considered when evaluating the PNASFH-Net using the CT images obtained from the CT colonography database [20].

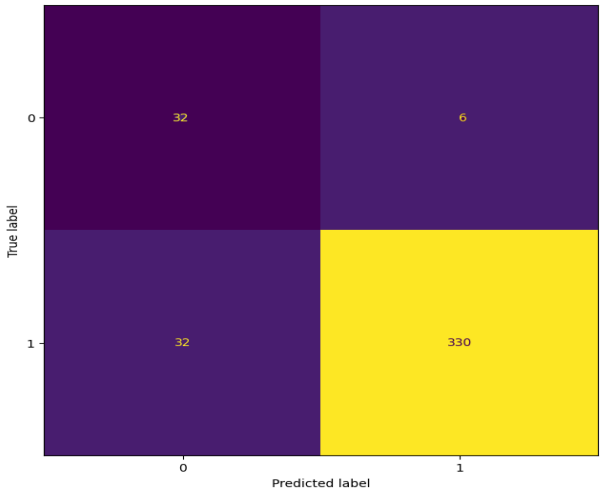

Figure 10. Confusion matrix of PNASFH-Net

3.10.1 Assessment based on training set

Figure 11 displays the examination of PNASFH-Net while evaluating different training set percentages. Figure 11a) displays accuracy-based valuation of PNASFH-Net. The existing methods, such as RSSOA-CNN based transfer learning, Vision transformer, DWWO-based deepRNN, CNN, Deep transfer learning, K-Means, and PNASFH-Net figured the accuracy value of 95.880%, 94.437%, 93.057%, 90.349%, 87.786%, 85.569%, and 98.167%, respectively, with a training set of 90%. The performance enhancement of PNASFH-Net is by 12.83%, 10.58%, 7.96%, 5.21%, 3.94%, and 2.33%. The evaluation of the PNASFH-Net in terms of sensitivity is shown in Figure 11b. When considering a training set of 90%, the PNASFH-Net attained a sensitivity value of 98.349% when compared to sensitivity values measured by the value of 95.785% for RSSOA-CNN-based transfer learning, 94.234% for Vision transformer, 93.785% for DWWO-based deepRNN, 90.786% for CNN, 88.755% for Deep transfer learning, and K-Means for 86.085%.

The performance of PNASFH-Net is improved by 12.47%, 9.76%, 7.69%, 4.64%, 4.36%, and 2.61%. The specificity-based analysis of PNASFH-Net is shown in Figure 11c. When considering the training set as 90%, PNASFH-Net computed a specificity of 98.025%, which is higher than the specificity of RSSOA-CNN based transfer learning, Vision transformer, DWWO-based deepRNN, CNN, Deep transfer learning, and K-Means at 94.182%, 93.079%, 91.567%, 88.980%, and 85.708%, respectively. The performance enhancement of PNASFH-Net is 14.36%, 10.16%, 7.05%, 5.31%, 4.07%, and 2.28%. The memory usage analysis of PNASFH-Net is shown in Figure 11d. When considering the training set as 90%, PNASFH-Net computed a memory usage of 98.025%, which is less than the memory usage of RSSOA-CNN based transfer learning, Vision transformer, DWWO-based deepRNN, CNN, Deep transfer learning, and K-Means at 58.5 MB, 58.4MB, 58.2MB, 58.1MB, 57.2MB, 56.9MB, and 56.6 MB, respectively.

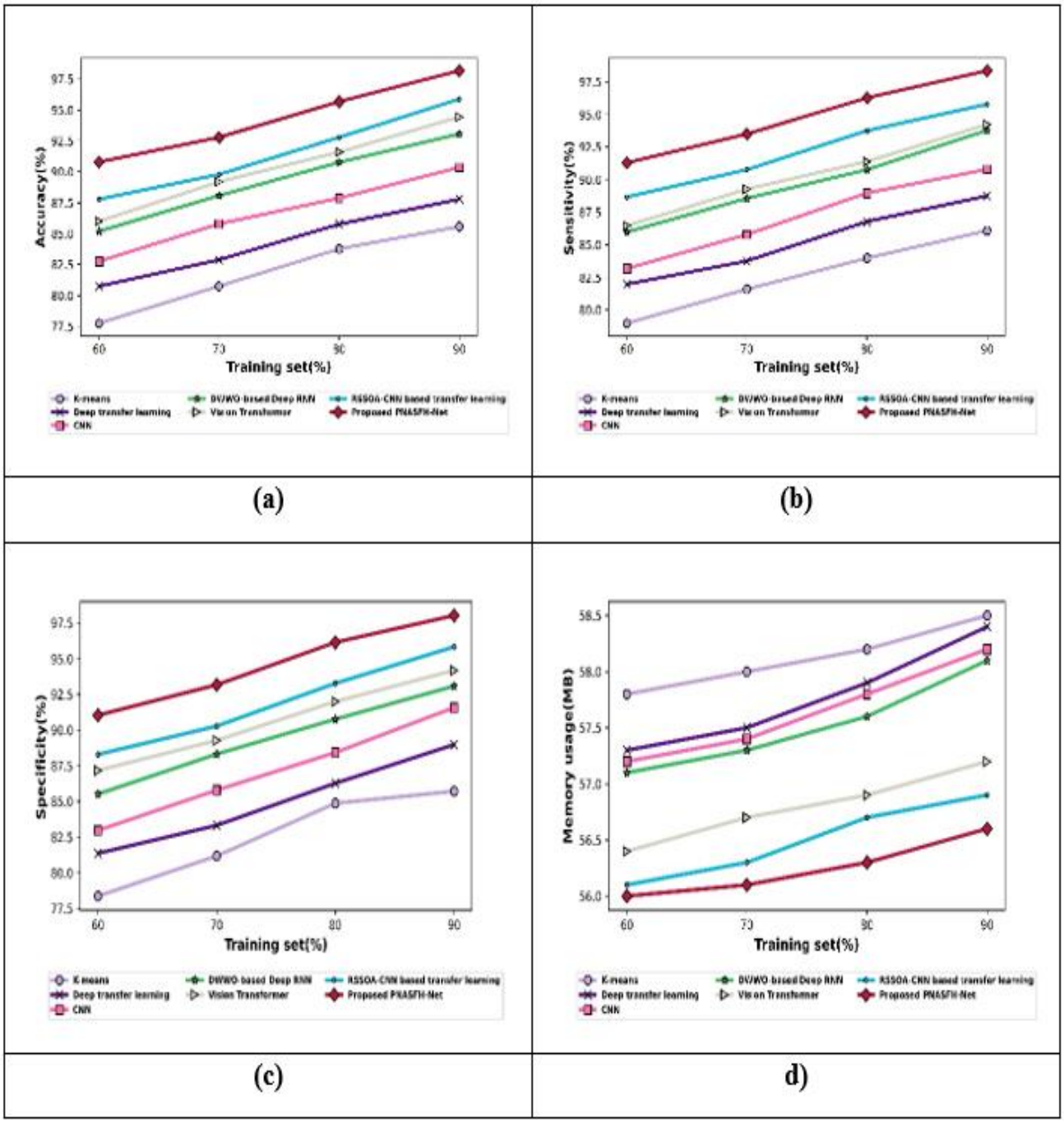

Figure 11. Investigation of PNASFH-Net using training set with respect to a) accuracy, b) sensitivity, c) specificity, and d) Memory usage

3.10.2 Assessment based on k-group

In Figure 12, the investigation of PNASFH-Net assessed using the K-group is illustrated. The accuracy-based evaluation of PNASFH-Net is demonstrated in Figure 12a. When considering the k-group is 9, the accuracy gained by RSSOA-CNN based transfer learning, Vision transformer, DWWO-based deepRNN, CNN, Deep transfer learning, K-Means, and PNASFH-Net is 96.005%, 95.172%, 93.190%, 92.178%, 90.789%, 87.988%, and 98.679%. The PNASFH-Net enhanced the performance by 10.53%, 7.68%, 6.27%, 5.24%, 3.33%, and 2.38%.

The Sensitivity-based assessment of the PNASFH-Net is displayed in Figure 12b. By considering K-group as 9, the sensitivity figured by PNASFH-Net is 98.679%, which is better compared to the sensitivity of RSSOA-CNN based transfer learning at 95.890%, Vision transformer at 94.276%, DWWO-based deepRNN at 93.990%, CNN at 92.199%, Deep transfer learning at 90.121%, and K-Means at 88.278%. The performance enhancement of PNASFH-Net is 10.54%, 8.67%, 6.57%, 4.75%, 4.66%, and 2.83%. Figure 12c displays the specificity-based investigation of PNASFH-Net. With k-group as 9, PNASFH-Net calculated a specificity value of 98.512%,

while RSSOA-CNN based transfer learning, Vision transformer, DWWO-based deepRNN, CNN, Deep transfer learning, K-Means values attained specificity of 95.948%, 94.276%, 93.540%, 92.089%, 90.399%, and 88.033%, correspondingly. The performance of PNASFH-Net is improved by 10.64%, 8.24%, 6.52%, 5.05%, 4.49%, and 2.60%. Figure 12d displays the memory-based investigation of PNASFH-Net. With k-group as 9, PNASFH-Net calculated a memory value of 56.8MB, while RSSOA-CNN based transfer learning, Vision transformer, DWWO-based deepRNN, CNN, Deep transfer learning, K-Means values attained memory of 57.1MB, 57.4MB, 58.2MB, 58.4MB, 58.6MB, and 58.5 MB correspondingly.

3.11 Ablation study

The ablation study on various evaluation metrics based on the training set and k-group is considered when evaluating the PNASFH-Net using the CT images obtained from the CT colonography database [20].

3.11.1 Assessment based on training set

Figure 13 displays the examination of PNASFH-Net while evaluating different training set percentages. Figure 13a displays the accuracy-based valuation of PNASFH-Net. The existing methods, such as CNN-based transfer learning, RSSOA-CNN-based transfer learning, NASNet, PCNN, and PNASFH-Net, achieved accuracy values of 94.956%, 95.879%, 96.278%, 97.237%, and 98.167%, respectively, with a training set of 90%.

The evaluation of the PNASFH-Net in terms of sensitivity is shown in Figure 13b. When considering a training set of 90%, the PNASFH-Net attained a sensitivity value of 98.348% when compared to sensitivity values measured by the value of 94.534%, for CNN-based transfer learning, 95.785%, for RSSOA-CNN-based transfer learning, 96.232% for NASNet, and 97.174% for PCNN. The specificity-based analysis of PNASFH-Net is shown in Figure 13c. When considering the training set as 90%, PNASFH-Net computed a specificity of 98.024%, which is higher than the specificities of CNN-based transfer learning, RSSOA-CNN-based transfer learning, NASNet, PCNN at 94.456%, 95.832%, 96.324%, and 97.287%, respectively.

3.11.2 Assessment based on k-group

Figure 14 displays the examination of PNASFH-Net while evaluating different training set percentages. Figure 14a displays the accuracy-based valuation of PNASFH-Net. The existing methods, such as CNN-based transfer learning, RSSOA-CNN-based transfer learning, NASNet, PCNN, and PNASFH-Net, achieved accuracy values of 95.287%, 96.005%, 96.324%, 97.003%, and 98.345%, respectively, with a training set of 90%. The evaluation of the PNASFH-Net in terms of sensitivity is shown in Figure 14b. When considering a training set of 90%, the PNASFH-Net attained a sensitivity value of 98.678% when compared to sensitivity values measured by the value of 94.474%, for CNN-based transfer learning, 95.889%, for RSSOA-CNN-based transfer learning, 97.178% for NASNet, and 97.993% for PCNN.

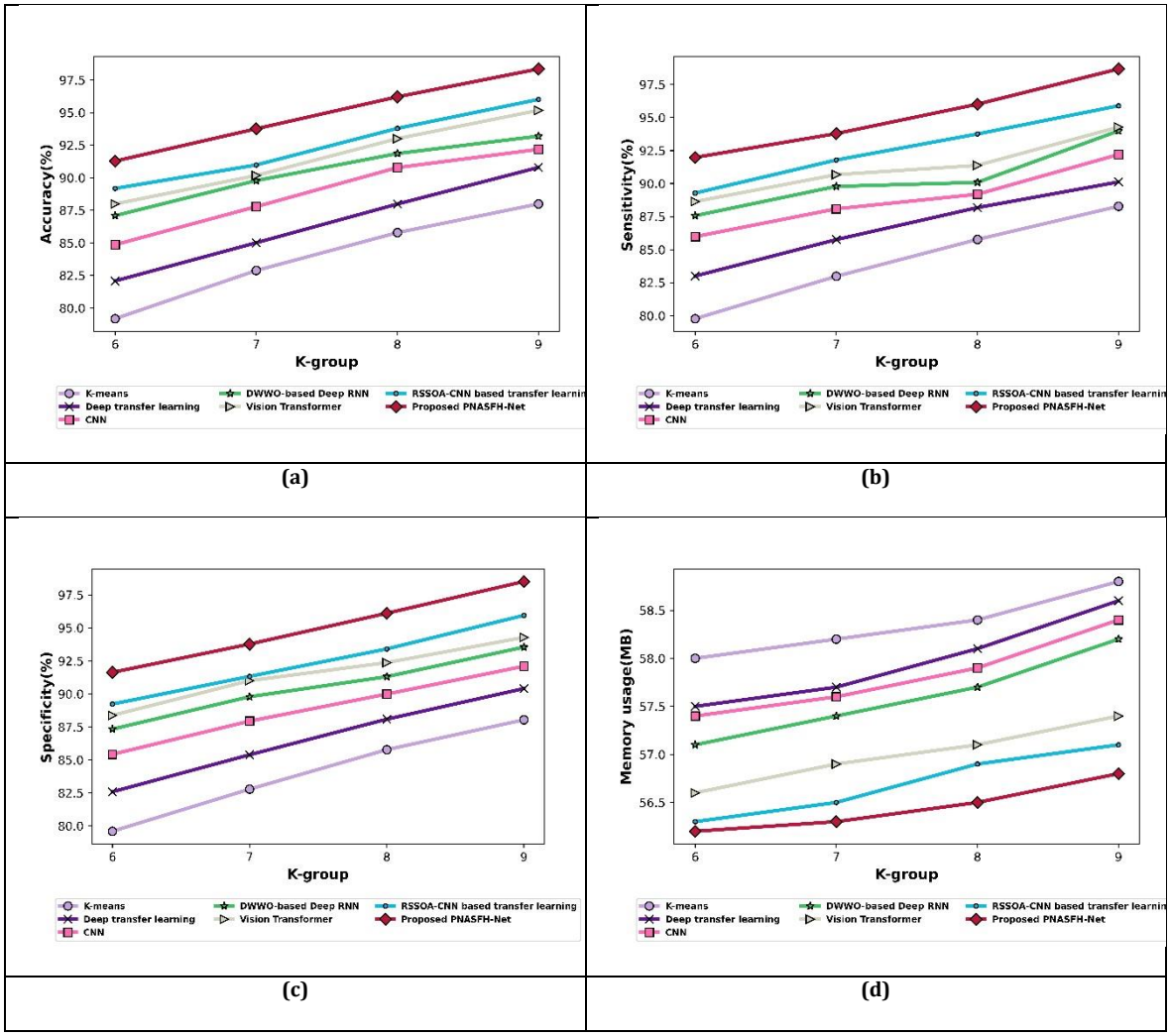

Figure 12. Examination of PNASFH-Net using k-group with respect to a) accuracy, b) sensitivity, c) specificity, and d) Memory usage

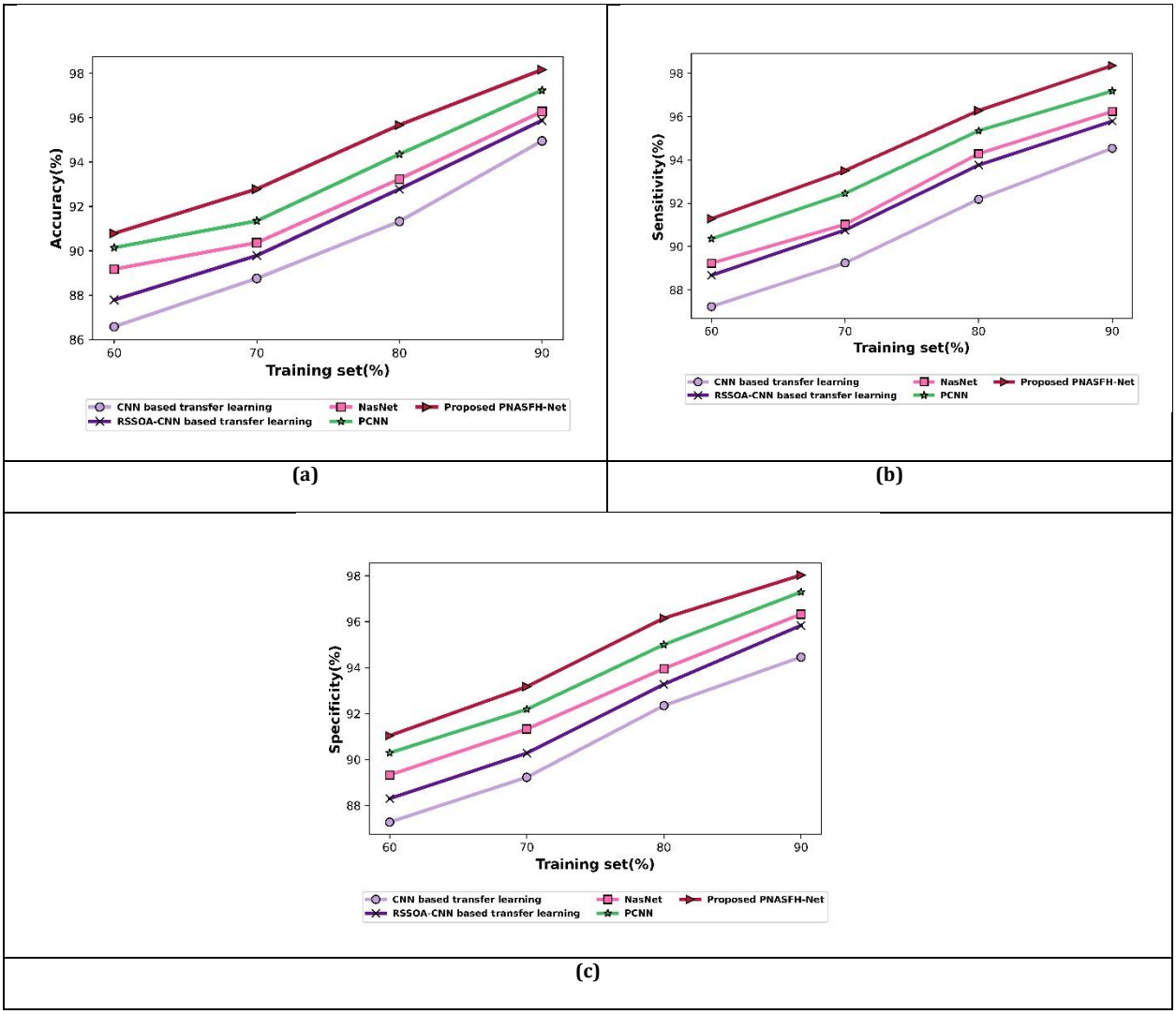

Figure 13. Ablation study analysis of PNASFH-Net using the training set with respect to a) accuracy, b) sensitivity, and c) specificity

Figure 14c shows the specificity-based analysis of PNASFH-Net. When considering the training set as 90%, PNASFH-Net computed a specificity of 98.512%, which is higher than the specificities of CNN-based transfer learning, RSSOA-CNN-based transfer learning, NASNet, and PCNN, which are 94.865%, 95.947%, 96.278%, and 97.454%, respectively.

4.11 Comparative discussion

The outcomes obtained by PNASFH-Net for colon cancer detection, as well as the results obtained by traditional colon cancer detection schemes, are depicted in Table 1. Here, superior detection performance is recorded by PNASFH-Net with a maximum of 98.345% accuracy, 98.679% sensitivity, 98.678% specificity, and 56.8MB memory usage for K-group 9. Moreover, the accuracy calculated by the approaches, such as RSSOA-CNN based transfer learning, Vision transformer, DWWO-based deepRNN, CNN, Deep transfer learning, K-Means is 96.005%, 95.172%, 93.190%, 92.178%, 90.789%, and 87.988%.

Similarly, the sensitivity attained by these conventional models is 95.890%, 94.276%, 93.990%, 92.199%, 90.121%, and 88.278%. Besides, specificity values of 95.889%, 94.276%, 93.989%, 92.198%, 90.120%, and 88.277% are attained by existing techniques, like RSSOA-CNN based transfer learning, Vision transformer, DWWO-based deepRNN, CNN, Deep transfer learning, K-Means. Moreover, memory values of 58.8MB, 58.6MB, 58.4MB, 58.2MB, 57.4MB, and 57.1MB are attained by existing techniques, like RSSOA-CNN-based transfer learning, Vision transformer, DWWO-based deepRNN, CNN, Deep transfer learning, K-Means. The PNASFH-Net, formed by combining PCNN with NASNet, obtained optimum outcomes. PCNN enhanced the computational power, while NASNet attained better generalizability and Harmonic analysis, and reduced the time complexity.

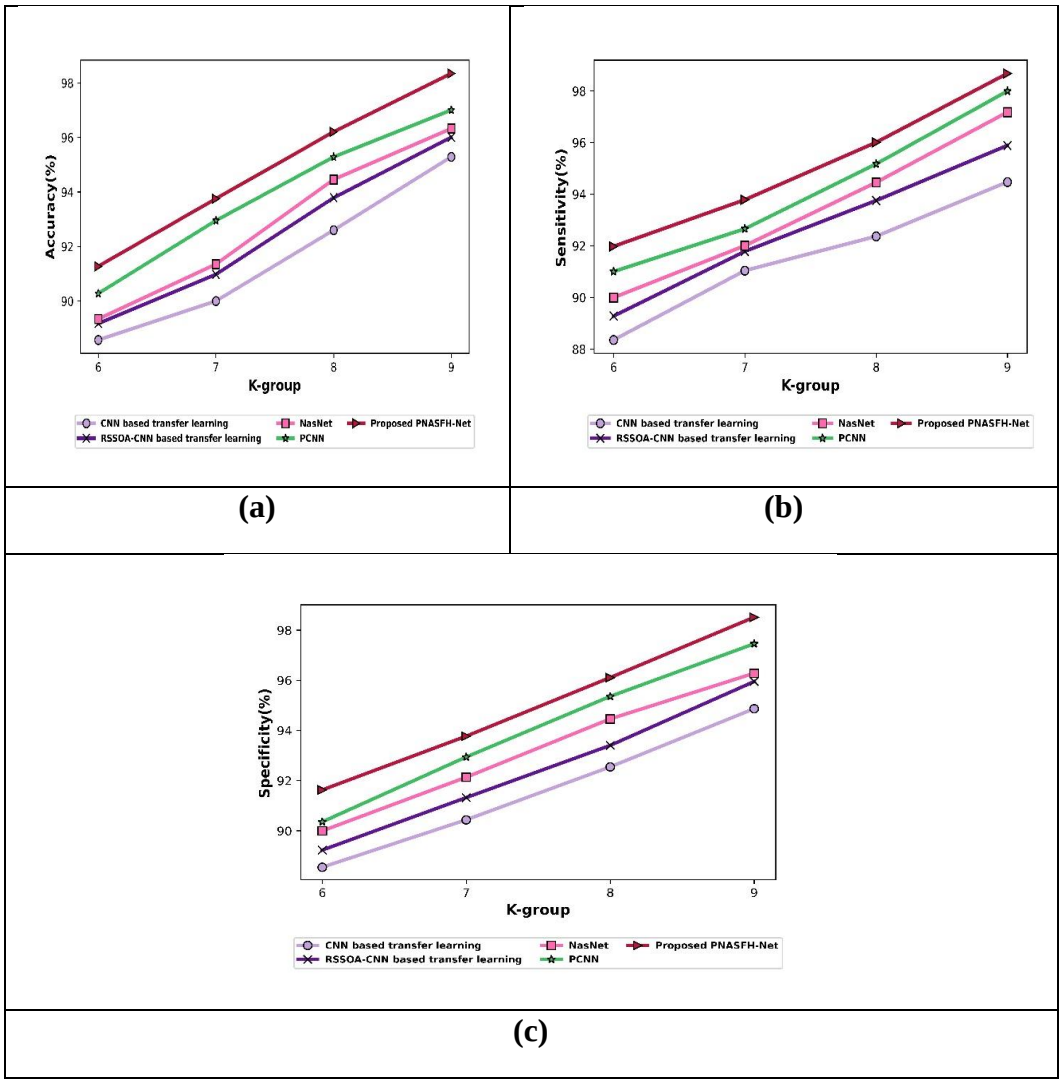

Figure 14. Ablation study analysis of PNASFH-Net using K-group with respect to a) accuracy, b) sensitivity, and c) specificity

Table 1. Comparative discussion of the PNASFH-Net model

Detection approaches	Performance metrics							
	Training set				K-group			
	Accuracy (%)	*Sensitivity (%)*	*Specificity (%)*	*Memory usage (MB)*	*Accuracy (%)*	*Sensitivity (%)*	*Specificity (%)*	*Memory usage (MB)*
K-means	85.569	86.085	85.708	58.5	87.988	88.278	88.033	58.8
Deep transfer learning	87.786	88.755	88.980	58.4	90.789	90.121	90.399	58.6
CNN	90.349	90.786	91.567	58.2	92.178	92.199	92.089	58.4
DWWO-based transfer learning	93.057	93.785	93.079	58.1	93.190	93.990	93.540	58.2
Vision transformer	94.437	94.234	94.182	57.2	95.172	94.276	94.276	57.4
RSSOA-CNN-based transfer learning	95.880	95.785	95.833	56.9	96.005	95.890	95.948	57.1
Proposed PNASFH-Net	98.167	98.349	98.025	56.6	98.345	98.679	98.512	56.8

5. Conclusion

DL techniques have been implemented for achieving high performance in identifying colon cancer when compared with other traditional ML approaches. Various approaches are exploited for detecting colon cancer but they are not efficient. Therefore, a new model termed as PNASFH-Net is formulated to detect colon cancer in its initial stage. For that, firstly, input colon image is pre-processed by employing AMF for eliminating the noise from the raw image. After that, the affected colon region is segmented by exploiting PNU-Net, which is tuned by using RSSOA. This RSSOA method is formulated by the amalgamation of SSOA and ROA. Following this, the features from the segmented image are mined, and finally, colon cancer detection is executed by using PNASFH-Net. Here, PNASFH-Net is engineered by the fusion of three techniques, such as Harmonic analysis, NASNet, and PCNN. Furthermore, the experimental outcomes of PNASFH-Net show that it computed an accuracy of 98.345%, specificity of 98.512%, sensitivity of 98.679%, and memory usage of 56.8MB correspondingly. The deployment of PNASFH-Net in clinical settings presents both challenges and opportunities. By addressing issues related to data integration, computational infrastructure, and clinician interpretability, and by considering ethical concerns surrounding patient privacy and accountability, healthcare providers can leverage AI to enhance diagnostic accuracy and improve patient outcomes. Future work should focus on developing robust frameworks for integrating AI into clinical workflows while ensuring that ethical standards are upheld. Also, to introduce feature selection methods for improving the accuracy rate by minimizing information loss and complexity.

Ethical issue

The authors are aware of and comply with best practices in publication ethics, specifically with regard to authorship (avoidance of guest authorship), dual submission, manipulation of figures, competing interests, and compliance with policies on research ethics. The author adheres to publication requirements that the submitted work is original and has not been published elsewhere.

Data availability statement

The manuscript contains all the data. However, more data will be available upon request from the authors.

Conflict of interest

The authors declare no potential conflict of interest.

References

[1] Saroja, B. and SelwinMich Priyadharson, A., "Adaptive pillar K-means clustering-based colon cancer detection from biopsy samples with outliers," Computer Methods in Biomechanics and Biomedical Engineering: Imaging & Visualization, vol.7, no.1, pp.1-11, 2019.

[2] Gessert, N., Bengs, M., Wittig, L., Drömann, D., Keck, T., Schlaefer, A. and Ellebrecht, D.B., "Deep transfer learning methods for colon cancer classification in confocal laser microscopy images," International journal of computer assisted radiology and surgery, vol.14, no.11, pp.1837-1845, 2019.

[3] Gessert, N., Wittig, L., Drömann, D., Keck, T., Schlaefer, A. and Ellebrecht, D.B., "Feasibility of colon cancer detection in confocal laser microscopy images using convolution neural networks," In Bildverarbeitung für die Medizin, Springer, pp. 327-332, 2019.

[4] Gupta, P., Huang, Y., Sahoo, P.K., You, J.F., Chiang, S.F., Onthoni, D.D., Chern, Y.J., Chao, K.Y., Chiang, J.M., Yeh, C.Y. and Tsai, W.S., "Colon tissues classification and localization in whole slide images using deep learning", Diagnostics, vol.11, no.8, pp.1398, 2021.

[5] Sakr, A.S., Soliman, N.F., Al-Gaashani, M.S., Pławiak, P., Ateya, A.A. and Hammad, M., "An efficient deep learning approach for colon cancer detection", Applied Sciences, vol.12, no.17, pp.8450, 2022.

[6] Kavitha, M.S., Gangadaran, P., Jackson, A., Venmathi Maran, B.A., Kurita, T. and Ahn, B.C., "Deep neural network models for colon cancer screening", Cancers, vol.14, no.15, pp.3707, 2022.

[7] Haq, I., Mazhar, T., Asif, R.N., Ghadi, Y.Y., Saleem, R., Mallek, F. and Hamam, H., "A deep learning approach for the detection and counting of colon cancer cells (HT-29 cells) bunches and impurities", PeerJ Computer Science, vol.9, pp.e1651, 2023.

[8] Obayya, M., Arasi, M.A., Alruwais, N., Alsini, R., Mohamed, A. and Yaseen, I., "Biomedical image analysis for colon and lung cancer detection using tuna swarm algorithm with deep learning model", IEEE Access, 2023 10.1109/ACCESS.2023.3309711.

[9] Qian, Y., "Removing of salt-and-pepper noise in images based on adaptive median filtering and improved threshold function", In proceedings of 2019 Chinese Control and Decision Conference (CCDC), pp. 1431-1436, IEEE, June 2019.

[10] Liu, C., Xie, H., Zhang, S., Mao, Z., Sun, J. and Zhang, Y., "Misshapen pelvis landmark detection with local-global feature learning for diagnosing developmental dysplasia of the hip", IEEE Transactions on Medical Imaging, vol.39, no.12, pp.3944-3954, 2020.

[11] Jia, H., Peng, X. and Lang, C.,"Remora optimization algorithm", Expert Systems with Applications, vol.185, pp.115665, 2021.

[12] Kaveh, A. and Zaerreza, A., "Shuffled shepherd optimization method: a new meta-heuristic algorithm", Engineering Computations, 2020 https://doi.org/10.1108/EC-10-2019-0481.

[13] Su, R., Liu, T., Sun, C., Jin, Q., Jennane, R. and Wei, L., "Fusing convolutional neural network features with hand-crafted features for osteoporosis diagnoses", Neurocomputing, vol.385, pp.300-309, 2020.

[14] Fan, K.C. and Hung, T.Y., "A novel local pattern descriptor—local vector pattern in high-order derivative space for face recognition", IEEE transactions on image processing, vol.23, no.7, pp.2877-2891, 2014.

[15] Davarzani, R., Mozaffari, S. and Yaghmaie, K., "Perceptual image hashing using center-symmetric local binary patterns", Multimedia Tools and Applications, vol.75, pp.4639-4667, 2016.

[16] Lee, S., Jha, D., Agrawal, A., Choudhary, A. and Liao, W.K., "Parallel deep convolutional neural network training by exploiting the overlapping of computation and communication", In proceedings of 2017 IEEE 24th international conference on high performance computing (HiPC), IEEE, pp. 183-192, December 2017.

[17] Cano, E., Mendoza-Avilés, J., Areiza, M., Guerra, N., Mendoza-Valdés, J.L. and Rovetto, C.A., "Multi skin lesions classification using fine-tuning and data-augmentation applying NASNe", PeerJ Computer Science, vol.7, pp.e371, 2021.

[18] Damsleth, E. and Spjøtvoll, E., "Estimation of trigonometric components in time series", Journal of the American Statistical Association, vol.77, no.378, pp.381-387, 1982.

[19] Martínez, F., Martínez, F. and Jacinto, E., "Performance evaluation of the NASNet convolutional network in the automatic identification of COVID-19", International Journal on Advanced Science, Engineering and Information Technology, vol.10, no.2, pp.662, 2020.

[20] CT colonography dataset is taken from "https://wiki.cancerimagingarchive.net/display/Public/CT+COLONOGRAPHY#e88604ec5c654f60a897fa77906f88a6 ", accessed on June 2024.

[21] Hamida, A.B., Devanne, M., Weber, J., Truntzer, C., Derangère, V., Ghiringhelli, F., Forestier, G. and Wemmert, C., "Weakly Supervised Learning using Attention gates for colon cancer histopathological image segmentation", Artificial Intelligence in Medicine, vol.133, pp.102407, 2022.

[22] Said, Y., Alsheikhy, A.A., Shawly, T. and Lahza, H., "Medical images segmentation for lung cancer diagnosis based on deep learning architectures", Diagnostics, vol.13, no.3, pp.546, 2023.

[23] Cifci, M.A., "Segchanet: A novel model for lung cancer segmentation in ct scans", Applied Bionics and Biomechanics, vol.2022, no.1, pp.1139587, 2022.

[24] Rathore, S., Hussain, M., Ali, A. and Khan, A., "A recent survey on colon cancer detection techniques", IEEE/ACM Transactions on computational biology and bioinformatics, vol. 10, no. 3, pp.545-563, 2013.

[25] Masud, M., Sikder, N., Nahid, A.A., Bairagi, A.K. and AlZain, M.A., "A machine learning approach to diagnosing lung and colon cancer using a deep learning-based classification framework", Sensors, vol.21, no.3, pp.748.

[26] Attallah, O., Aslan, M.F. and Sabanci, K., "A framework for lung and colon cancer diagnosis via lightweight deep learning models and transformation methods", Diagnostics, vol.12, no.12, pp.2926, 2022.

[27] Pavan Kumar , V. T. R. ., Arulselvi, M., & Sastry, K. B. S. (2023). Comparative Assessment of Colon Cancer Classification Using Diverse Deep Learning Approaches. Journal of Data Science and Intelligent Systems, 1(2), 128-135 https://doi.org/10.47852/bonviewJDSIS32021193